LONG-PERIOD CYCLES OF THE SUN'S ACTIVITY RECORDED IN DIRECT SOLAR DATA AND PROXIES

M. G. OGURTSOV[1], YU. A. NAGOVITSYN[2], G. E. KOCHAROV[1] and H. JUNGNER[3]
[1]*A.F. Ioffe Physical-Technical Institute, 194021, Polytechnicheskaya 26, St.-Petersburg, Russia*
(e-mail: maxim.ogurtsov@pop.ioffe.rssi.ru)
[2]*Pulkovo Astronomical Observatory, 196140, Pulkovskoe shosse 65/1, St.-Petersburg, Russia*
(e-mail: nag@gao.spb.ru)
[3]*University of Helsinki, P.O. Box 64, FIN-00014, Gustaf Hällströminkatu 2, Helsinki, Finland*

(Received 4 June 2002; accepted 6 August 2002)

Abstract. Different records of solar activity (Wolf and group sunspot number, data on cosmogenic isotopes, historic data) were analyzed by means of modern statistical methods, including one especially developed for this purpose. It was confirmed that two long-term variations in solar activity – the cycles of Gleissberg and Suess – can be distinguished at least during the last millennium. The results also show that the century-type cycle of Gleissberg has a wide frequency band with a double structure consisting of 50–80 years and 90–140 year periodicities. The structure of the Suess cycle is less complex showing a variation with a period of 170–260 years. Strong variability in Gleissberg and Suess frequency bands was found in northern hemisphere temperature multiproxy that confirms the existence of a long-term relationship between solar activity and terrestial climate.

1. Introduction

It is well known that the Sun actively influences many phenomena on the Earth. Due to this link, changes of solar activity affect many aspects of the life of mankind. The question about the role of solar variability in global climate change today is of special interest. Therefore, knowledge of the history of solar activity, its time evolution and its documentation in solar-terrestrial relationship is of great importance. It is evident that such knowledge needs reliable information on the time behavior of different parameters of solar activity (SA) over maximally long times. However, we have reliable information on SA (direct observations of a global magnetic field of the Sun, measurements of galactic cosmic ray intensity and fluxes of solar radiation in different spectral ranges) only for the last few decades. The knowledge of SA during the last 100–150 years (Zürich series of Wolf numbers, Greenwich series of sunspot area, *Aa* and *Kp* geomagnetic indices) is poorer. Tremendous work, done by Wolf and Waldmeier (1961), Hoyt and Schatten (1998), who compiled a lot of sporadic sunspot observations of 17th to the beginning of 19th centuries, allowed to obtain a reconstruction of sunspot numbers over the last 3–4 centuries. The reliability of these reconstructions before the middle of 19th century needs further investigation. Data on SA over longer time intervals can be obtained only from solar proxies (historical data, cosmogenic isotopes) and hence are substantially

Solar Physics **211:** 371–394, 2002.

less reliable. But in spite of the limited length of records of SA, some modes of long secular solar variability are already known. In the second half of the 19th century Wolf suggested solar cycles with periods of 55 and 160 years (see Schove, 1983). In the following century the ideas of Wolf were developed and significant evidence of the existence of two longer periodicities of SA were obtained. The first of them is a century-scale cycle revealed by Gleissberg (1944). Usually this cycle is considered as a variation with the period 80–90 years or, sometimes, even precisely 88 year. The second one is a variation with a period of about 200 (160–270) years (Schove, 1983). This is often called a Suess cycle. Suess (1980) found a significant 203 year variation in tree-ring radiocarbon records. It should be noted, however, that there are many evidences that the century-type solar variability may have spectral power in a wider frequency band than 80–90 years. For example in the work of Cole (1973), the double structure of the century-type cycle was found both for Zürich sunspot data (59 and 88 year) and for data on the phase of the 11-year solar cycle (78.5 and 94.5 year). Wittmann (1978) found 92-year and 55-year peaks in the spectrum of yearly averaged sunspot numbers for AD 1701–1976. Spectral analyses of the data on aurora borealis after 500 A.D. show peaks at 58 year and 65 year and a broad peak in the range 80–130 years (Schowe, 1983). Stuiver and Braziunas (1993) analyzed the long decadal ^{14}C series and found significant 89 and 148 year periodicities for 6000–2000 B.C. and a 126-year variation for 2000 B.C.–1840 A.D. Existence of two kinds of century-long solar variability – 115 year and 95 year cycles – was claimed by Chistyakov (1986). A thorough investigation of solar centennial variability over a long time scale was done by Nagovitsyn (1997, 2001). He used historic data and showed that the length of the century-long solar cycle is not constant and most likely changes from about 65 to more than 130 years (the 70–80-year and 100–120-year modes dominate).

In the present work we continue the analyses of long-term (20–300 years) SA variations in the Gleissberg and Suess frequency range, using all the complexity of direct and indirect solar data and applying modern statistical methods. The link between solar activity and terrestrial climate is also considered.

2. Data

In order to trace the long-term solar variability in detail we used all available data on SA direct oberservations and different proxies.

2.1. Direct data on solar activity

2.1.1. *Telescopic Sunspot Observations*

Despite the first accurate description of sunspots made by Kepler in 1607, systematic and qualified telescopic observations of sunspots begin only at the middle of the 19th century. But strong efforts of many scientists, and particularly of Rudolf

Wolf (director of the Observatory at Bern and later in Zürich) make it possible to extend the sunspot record back to the beginning of 18th century. The reliability of different parts of the Wolf number data set, however, is different: the data are reliable since 1848, their reliability is good during 1818–1848, it is questionable from 1749–1817 and it is poor during 1700–1748 (Eddy, 1976). Recently Hoyt and Schatten (1998) have finished the reconstruction of group sunspot number (GSSN) in which they used many historical sources missed by previous investigators. Their data set covers the time interval 1610–1995 and authors consider GSSN data as quite reliable during 1653–1730, 1750–1788 and after 1795 (Hoyt and Schatten, 1998). Wolf numbers and GSSN show some differences in the 18th century – the values of Wolf numbers during this period are a bit higher. These two series are the longest direct instrumental records of SA.

2.1.2. *Historical Naked-Eye Sunspot Observations*

The largest sunspots and sunspot groups (a total area more than 1900 μh) can be seen with unaided eye at sunrise and sunset or through smoke and haze (Wittmann, 1978). These sunspots were observed during the pre-telescopic era by ancient Oriental (in particularly Chinese) astronomers and now the data on ancient sunspot observations made by naked eye (SONE) is the longest non-proxy record of SA in the past. The most complete catalogue of SONE, covering more than 18 centuries and including more than 200 events, was collected by Wittmann and Xu (1987). The reliability of the information on solar activity, extracted from historical chronicles, was analysed in many works (see Willis, Easterbrook, and Stephenson (1980), Wittmann and Xu (1987), Nagovitsyn (2001)) and it was shown that the Oriental historic data really reflect such features of sunspot activity as 11-year and century-scale cycles, butterfly diagrams, deep Maunder-type minima of SA. Qualification of ancient Chinese astronomers also was high – observations of many lunar and solar eclipses, novae, supernovae, comets, meteor showers and even a possible observation of Jupiter's satellite Ganymede (364 B.C.) confirm their professionalism. However, the SONE record have substantial shortcomings:

(1) It is very likely that ancient astronomers often mixed real sunspots with other celestial or meteorological phenomena. For example, Wittmann and Xu (1987) compared more than 20 Oriental sunspot sightings with the data of European astronomers since 1848 and they found that only one third of the naked-eye observations are confirmed by western telescopic records.

(2) Ancient sunspot observations were not systematic and, as a result, are non-uniform in time. For example, very often sunspots were detected near the day of new moon. This happened because just in these periods observations were more frequent and intensive – determination of the new moon date had an important calendar purpose (Wittmann and Xu, 1978). Dating of observations is also not always quite accurate.

(3) Some climatic effects may be present in different SONE series (Willis, Easterbrook, and Stephenson, 1980). Nevertheless, SONE data are rather valuable

for investigation of solar variability over a long time scale and the catalogue of Wittmann and Xu was intensively used in our work.

2.2. Solar activity proxies

2.2.1. *Cosmogenic Isotope ^{10}Be*

The cosmogenic isotope ^{10}Be is generated in the Earth's atmosphere in reactions of secondary component of galactic cosmic rays (GCR) with the nuclei ^{14}N and ^{16}O. After its generation ^{10}Be is oxidised to BeO, captured by atmospheric aerosols, removed from atmosphere by precipitation (the atmosphere residence time is 1–2 years (Beer *et al.*, 1990)) and finally fixed in polar ice and bottom sediments. The concentration of beryllium in polar ice is directly influenced by the intensity of GCR. Because high-density magnetic regions of solar wind, which affect scattering and transport of GCR in the heliosphere, are governed by activity of the Sun, the intensity of GCR is well controlled by SA. Therefore ^{10}Be concentration in ice contains important information about SA in the past. Investigations of past SA activity based on ^{10}Be data have been presented in many works (Beer *et al.*, 1990, 1994). It has been shown that records of cosmogenic beryllium clearly report SA. It should be noted, however, that the concentration of beryllium in ice depends not only on GCR intensity but on the rate of ice accumulation. This feature determines the main shortcoming of the ^{10}Be record – its dependence on local climate, in particular via precipitation rate (see, e.g., Lal, 1987; Monaghan, 1987; Beer *et al.*, 1988; Damon and Peristykh, 1997). In the present work we used the data on ^{10}Be concentration in the South Pole ice. The record was obtained by Bard *et al.* (1997) and covers the time interval after A.D. 850.

2.2.2. *Cosmogenic Isotope ^{14}C*

The cosmogenic isotope ^{14}C is produced in the atmosphere by the reaction of cosmic-ray-induced thermal neutrons with nitrogen ^{14}N(n, p)^{14}C. Then ^{14}C is oxidized to CO_2 and assimilated into a number of geochemical and geophysical processes and distributed between the main carbon reservoirs (atmosphere, biosphere, ocean). Records of radiocarbon concentration in the past are mainly based on measurements of ^{14}C concentration in tree rings. The ability of ^{14}C to reflect long-term changes of SA has been established many years ago (see, for example, Stuiver and Braziunas, 1989). The basic problems with the use of radiocarbon data are the following:

(1) As in the case of beryllium, the concentration of ^{14}C in tree-rings is sensitive not only to changes of activity of the Sun but also to changes of climate (Damon, 1970; Stuiver and Braziunas, 1993; Peristykh and Damon, 2000).

(2) The carbon exchange system works as a low-pass filter, which attenuates the short-term variations of the rate of radiocarbon production Q and amplifies long-term changes. This results in essential deformations of primary variations of Q (and hence of GCR intensity) obtained from radiocarbon tree-ring records.

A well-known way to overcome the second difficulty is to use not $\Delta^{14}C$ data but a value Q, reconstructed by means of a many-reservoir carbon exchange system. However, the value of the reconstructed radiocarbon production rate substantially depends on the rate of exchange between different carbon reservoirs (see, for example, Stuiver and Quay, 1980). In the present work we therefore used the extended, decadal $\Delta^{14}C$ record derived from tree-rings (Stuiver and Pearson, 1993), covering the time interval back to 7950 BP. This is the one of the longest S.A. proxies existing today. It should be noted that GCR intensity is controlled by interplanetary magnetic field and the sunspot number is not a very precise indicator of this field. For example, Solanki, Schüssler, and Fligge (2000) have shown that the time-averaged level of interplanetary magnetic flux depends on the Schwabe (11 year) cycle length, too. So, the concentration of both cosmogenic isotopes (^{14}C and ^{10}Be) in natural archives likely reflects mainly the solar modulation of heliospheric conditions.

2.2.3. *Historical Auroral Observation*

Aurora borealis is a result of fluorescence of ionized atmospheric gases, mainly nitrogen. This ionization is caused by currents in the upper atmosphere, which in turn are results from the interaction of solar wind with the Earth's magnetosphere. Hence, the frequency of aurorae occurrences is closely connected with the activity of the Sun. The polar lights are easily observed by the unaided eye and for this reason we have historical information on auroral activity up to two thousand years back. Schove (1979) has determined dates of maxima of the 11-year solar cycles and estimated approximate Wolf numbers at each maximum during more than 2000 years using catalogues of ancient auroral observations and some preliminary assumptions. Nagovitsyn (1997), in turn, reconstructed Wolf numbers for A.D. 1100–1700 using the data of Schove and a specially developed nonlinear model of solar cyclicity. Obviously, the reconstruction made by Nagovitsyn is really a proxy of auroral activity rather than SA. It should be noted that these data substantially overestimate SA in periods of its deep minima. For example, Wolf numbers, derived from auroral observations, reach a value of 20–30 during the Maunder minimum. This is probably connected with the attenuation of a link between sunspot activity and aurorae in very low activity epochs.

All the proxies, used in our analysis (filtered or averaged), are plotted in Figure 1 together with data on historic minima and maxima of SA established by Eddy (1976) and Schove (1983). The similarity between long-term variations of all these SA indicators is quite evident and can be taken as proof for the reliability of the chosen proxies.

2.3. Climatic proxies

Methods of dendrochronology, intensively developed lately, allow reconstructing 40–60% of the variance of the temperature signal. In the present work, we used

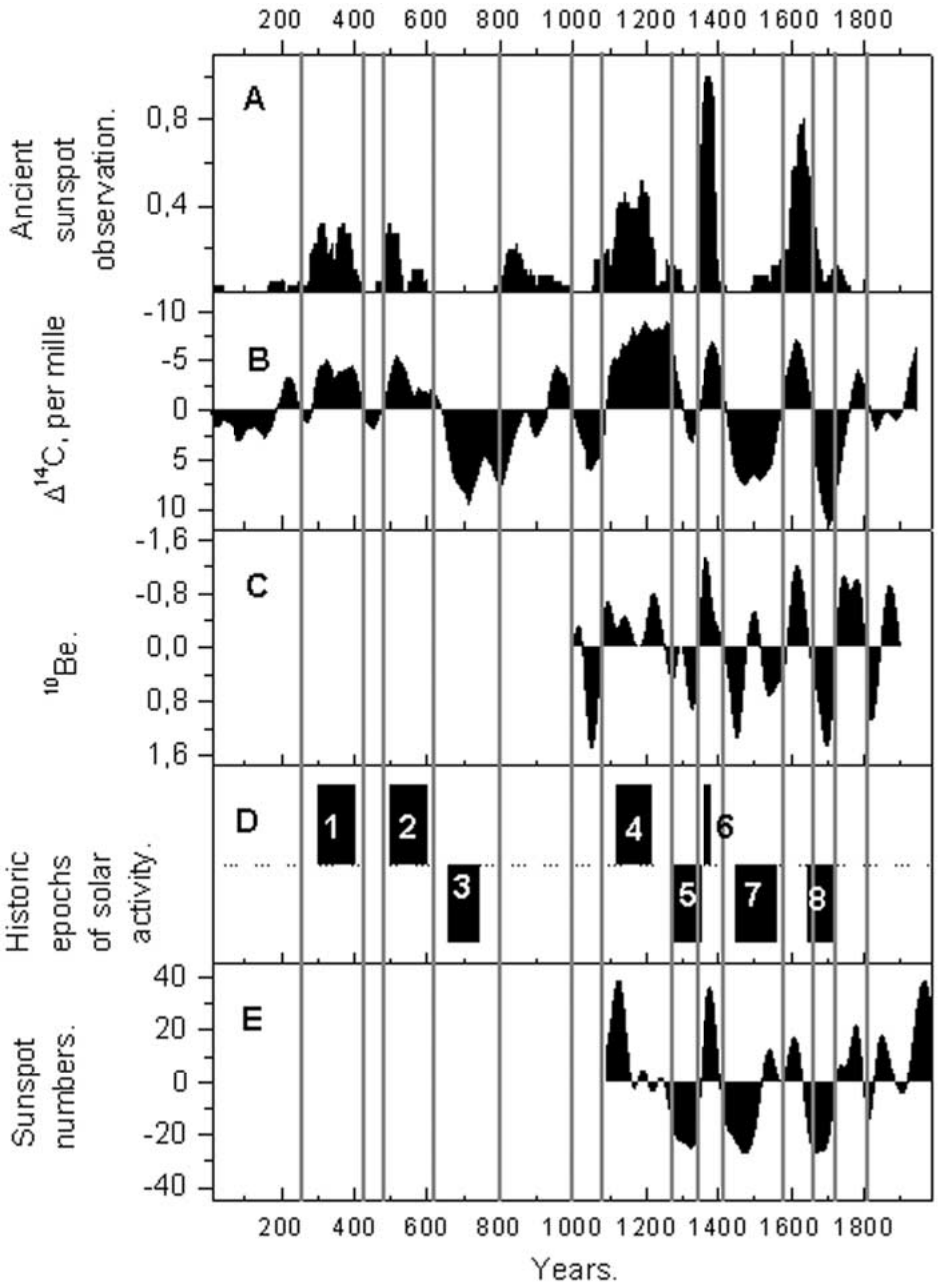

Figure 1. (A) Number of sunspot observations made by the naked eye (35 year averaged)). (B) Band-pass filtered decadal $\Delta^{14}C$ data. (C) Data on ^{10}Be at South Pole (relative fluctuation), wavelet filtered in 64–128 scale band. (D) Historic maxima and minima of solar activity: (1) Late Roman maximum, (2) Byzantine maximum, (3) Dark Age minimum, (4) Medieval maximum, (5) Wolf minimum, (6) Late Medieval maximum, (7) Spoerer minimum, (8) Maunder minimum. (E) Reconstructed Wolf numbers, wavelet filtered in 64–128 scale band.

tree-ring reconstruction of mean annual temperature in the northern hemisphere (Mann, Bradley, and Hughes, 1999) to show a possible solar–climate link over the last millennium.

3. Methods

The main aim of the present work was to analyse the spectral content of SA and its evolution in time. For this reason a complex analysis using both Fourier and wavelet approaches was performed. The basic properties of Fourier and wavelet transforms and the advantage of the wavelet one in the analyses of non-stationary time series have been described in many works (see, for example, Astafieva, 1996; Torrence and Compo, 1998; Ogurtsov *et al.*, 2001). We note that in the present work as in the previous one by Ogurtsov *et al.* (2001) we used the Morlet basis for the time-spectral analysis and the MHAT basis for filtration. One of the more important problems of wavelet analysis is the determination of confidence levels for local and global wavelet spectra. In this work we solved this problem using a method described in Appendix 1.

In order to analyse the significance of both Fourier and wavelet spectra we must know the value of factor α of red (AR (1)) noise present in the data. These factors were estimated by means of the following procedure. First, the low-frequency component (usually with periods more than 50 years) were filtered out of the series under investigation $y(t)$ and the residual part $y^{\mathrm{res}}(t)$ was considered as consisting mainly of noise. Secondly, the function $y^{\mathrm{res}}(t) = \alpha^* y^{\mathrm{res}}(t-1)$ was constructed and α was estimated. Numerical experiments, made with artificial data sets, show that this method allows the determination of the factor AR(1) with uncertainty less than 20%.

Analysis of SONE data is another serious problem. The quality of information, contained in Oriental chronicles is not good enough to use them for accurate quantitative estimations of SA level. Therefore we converted SONE data into a binary form: $S(t) = 1$ if an event (sunspot) was recorded in year t, $S(t) = 0$ if an event was not recorded. But statistical analysis of such binary series is not easy, because the majority of statistical methods cannot be applied in that case. Therefore, we searched for the characteristic periodicities in SONE data using an approach of autosimilarity functions, especially carried out for this purpose and described in Appendix 2.

4. Results and Discussion

In Figure 2 the local Morlet wavelet spectra of GSSN (Figure 2(a)) and Wolf numbers (Figure 2(b)) are presented. The spectra were calculated for the same time interval A.D. 1700–1995 and the 0.99 confidence level (c.l.) was evaluated in

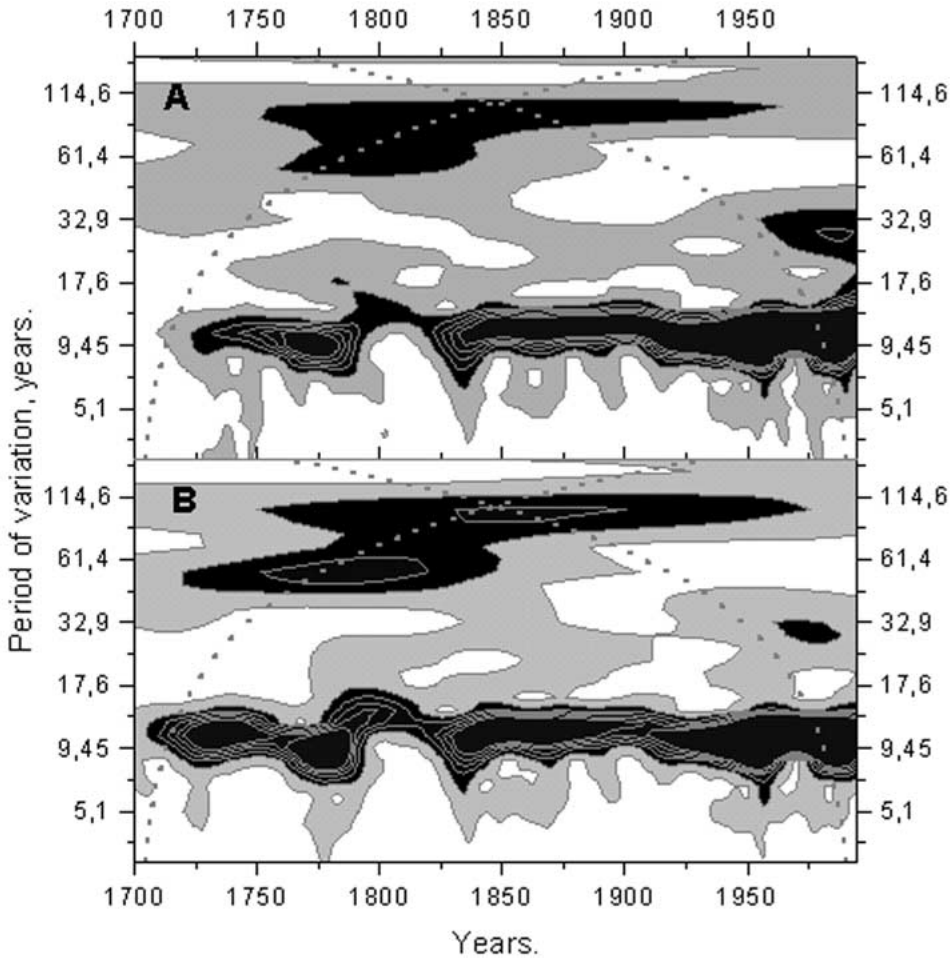

Figure 2. (A) Local wavelet (Morlet basis) spectrum of GSSN. *White domains* – local wavelet power < 0.2, *black domains* – local wavelet power > 1.0 (0.99 c.l.), step of local wavelet power – 0.8. (B) Local wavelet (Morlet basis) spectrum of Wolf numbers. *White domains* – local wavelet power < 0.2, *black domains* – local wavelet power > 1.0 (0.99 c.l.).

assumption about red noise with $\alpha = 0.3$. It is seen from Figure 2 that two significant century-scale oscillations really are in the spectrum of sunspot variability, a 90–100-year cycle (since the second part of the 18th century) and 50–60-year cycle (until the first part of the 19th century). The shorter cycle is manifested more clearly in Wolf numbers. So, both series, Wolf numbers and GSSN, show the bimodal structure of century-long variation. However, instrumental records are too short to make more precise conclusions about the character of centennial solar variability and its time evolution.

A much longer SONE series was analysed using the approach of autosimilarity function (see Appendix 2). For a more convenient analysis, the series, covering

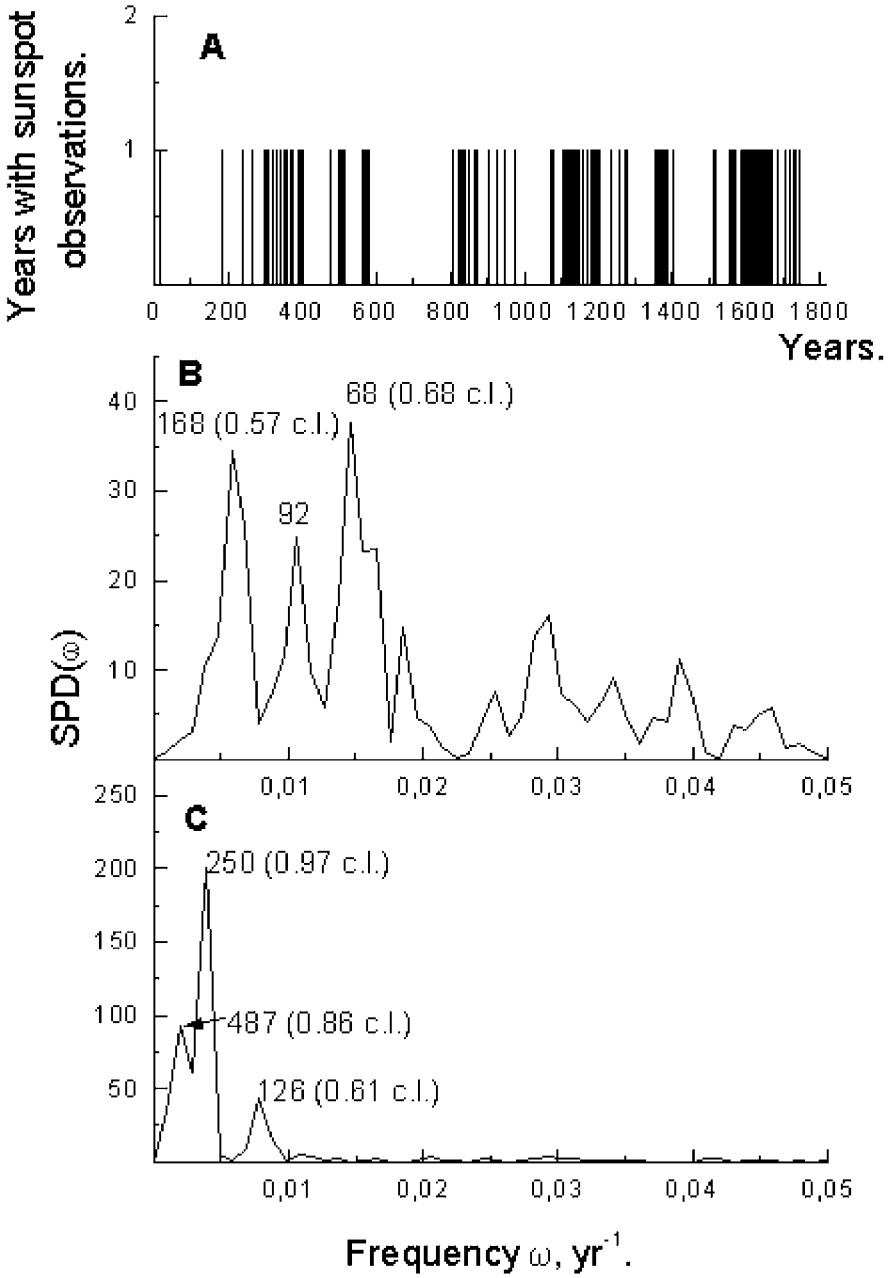

Figure 3. (A) Binary SONE data. (B) Fourier spectrum of the autosimilarity function of binary SONE data for 0–600 A.D. (C) Fourier spectrum of the autosimilarity function of binary SONE data for 801–1801 A.D.

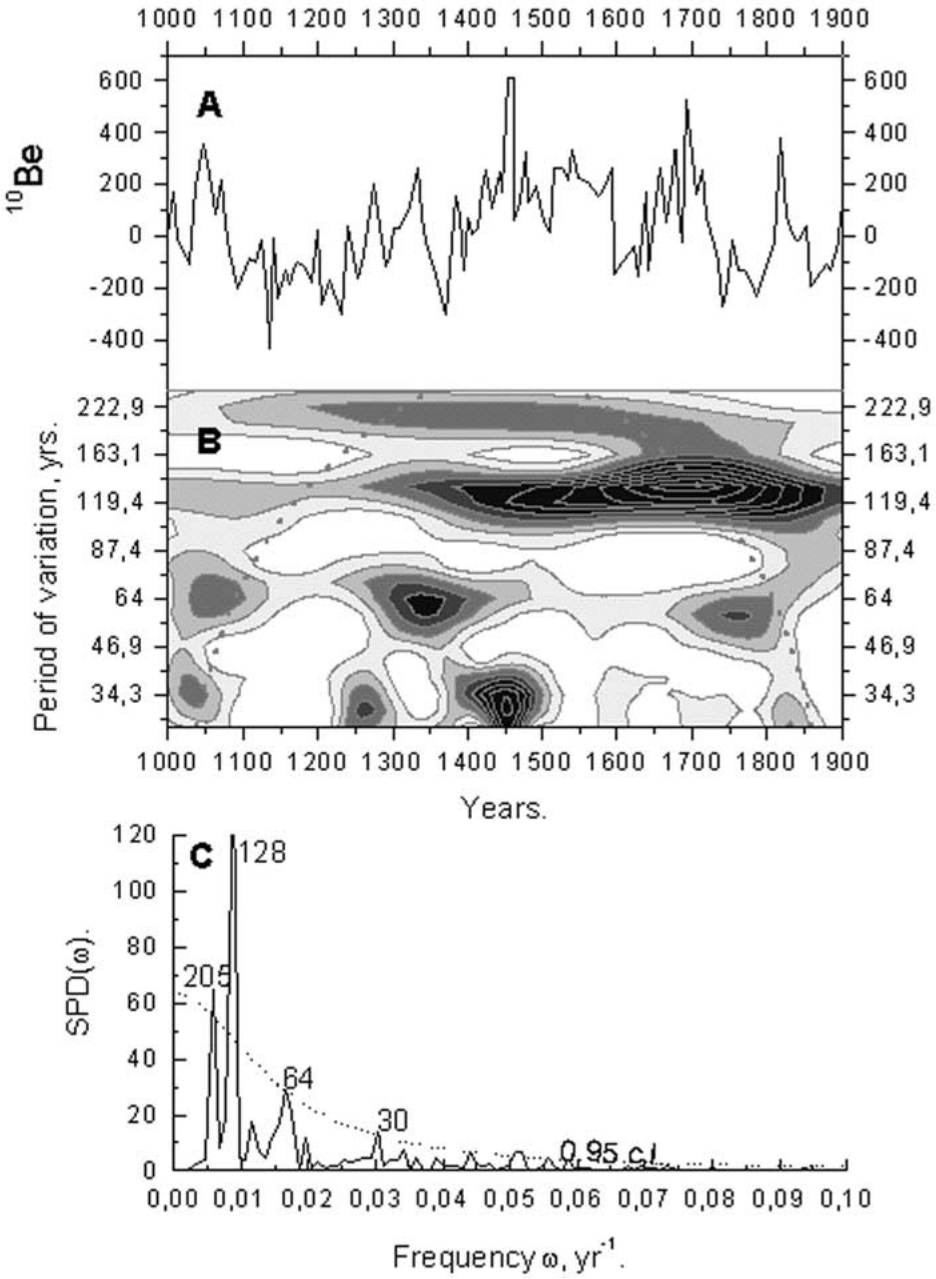

Figure 4. (A) ^{10}Be concentration in South Pole ice (see Figure 1 in Bard *et al.* (1997)). (B) Local wavelet (Morlet basis) spectrum of ^{10}Be concentration. *White domains* – local wavelet power < 0.2, *black domains* – local wavelet power >1.0 (0.99 c.l.). (C) Fourier spectrum of ^{10}Be concentration. *Dotted line*: 0.95 c.l. (red noise factor 0.9).

time interval A.D. 0–1800, was divided into two parts: 0–600 A.D. and 801–1801 A.D. Fourier spectra of autosimilarity functions of both these data sets are plotted in Figure 3. Significances of the main peaks in the spectra were estimated using a statistical experiment, described in Appendix 2. It is seen from Figure 3 that the significance of the majority of the spectral peaks is low. This is likely a result of the non-systematic character of the observations and a lot of noise input by ancient astronomers, who often mixed sunspots with other phenomena, into their record. Nevertheless, this series contains some information about solar variability in the Suess and Gleissberg frequency bands. The 250-year cycle is distinctly manifested in SONE data after AD 800 (c.l. $> 2\sigma$) and before AD 800 the 170-year periodicity is present, though weak. This result is in agreement with that obtained by the Yunnan group (1977), who analysed the medieval Chinese sunspot observations and suggested two cycles in their data – the stronger at 240–270 years and a weaker one at 165–210 years. Century-scale variability of SONE data is manifested by peaks at 68, 92, and 126 years, though the more significant of them (68 years) attains only 1σ c.l. Cycles with periods of 61 years and 81–91 years were also found in the Yunnan Observatory (1977). Ancient Oriental sunspot observations thus confirm the existence of the Suess cycle and give evidence that century-scale solar variability has a wide frequency band (60–130 years). More exhaustive analysis of SONE data can be found in the work of Nagovitsyn (2001).

A long beryllium record from Antarctica (Bard *et al.*, 1997) (A.D. 1000–1900, Figure 4(a)) was analysed using both wavelet and Fourier approaches. The factor of red noise was estimated as 0.9, and spectra of ^{10}Be data (local wavelet and Fourier ones) are shown in Figures 4(b) and 4(c). It is seen from Figure 4 that ≈ 200 years, 110–135 years and 50–70 years variations are present in the beryllium series during almost all time intervals. The second oscillation mode is the strongest while the significances of the other two cycles are not so high.

A reconstruction of Wolf numbers made by Nagovitsyn (1997) using SA estimations made by Schove (who, in turn, mainly used auroral data) is shown in Figure 5(a). Together with the direct Wolf numbers the series covers the time interval A.D. 1100–1995. The record was analysed in the same way as the previous record. Wavelet and Fourier spectra, plotted in Figure 5, show the presence of highly significant periodicities in the periods of 170–220, 90–135, and 50–85 years. The Suess cycle is the most significant. The factor of red noise was 0.3.

Finally, we investigated the decadal radiocarbon series of Stuiver and Pearson (1993). For convenience of analysis, we constructed a series of residuals of the Δ^{14}C record from the initial data set filtered in a 80–1000 year band. This data set is presented in Figure 6(a). Then, as in the previous cases, Fourier and wavelet analyses were been performed. The results are shown in the Figures 6(b) and 6(c). As seen in Figure 6, the radiocarbon spectrum also shows variance in 160–270-year, 80–140-year, and 40–70-year bands. These cycles are strongest during 2500–6000 B.C. (see Figure 6(b)). It is known that the time interval 2500–6000 B.C. was a period of a weak geomagnetic dipole field, which shields the Earth from

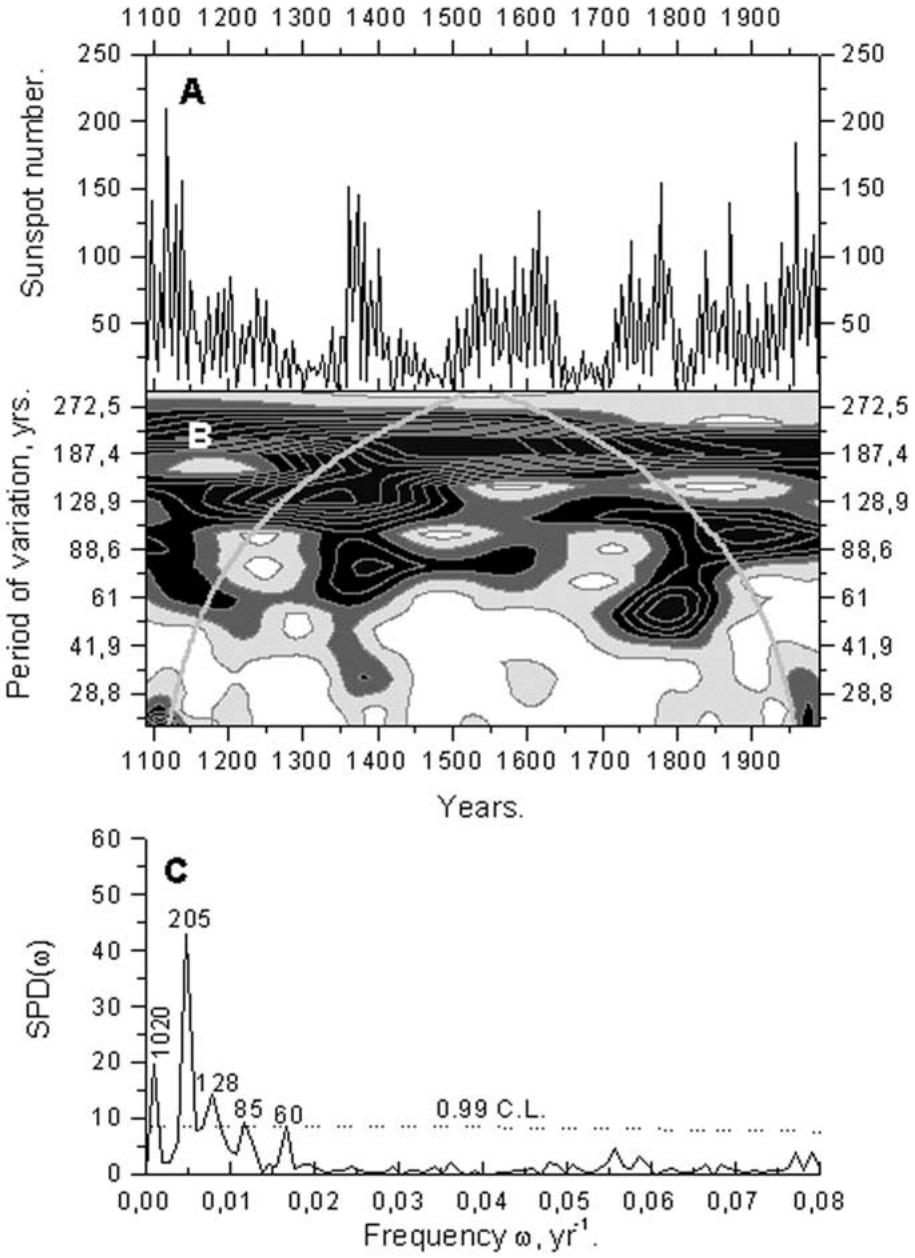

Figure 5. (A) Wolf numbers reconstructed by Nagovitsyn (1997) using data of Schove (1979). After 1700 A.D. – direct Zürich data. (B) Local wavelet (Morlet basis) spectrum of Wolf numbers reconstructed by Nagovitsyn. *White domains* – local wavelet power < 0.2, *black domains* – local wavelet power > 1.0 (0.99 c.l.). (C) Fourier spectrum of Wolf numbers reconstructed by Nagovitsyn. *Dotted line*: 0.99 c.l. (red noise factor 0.3).

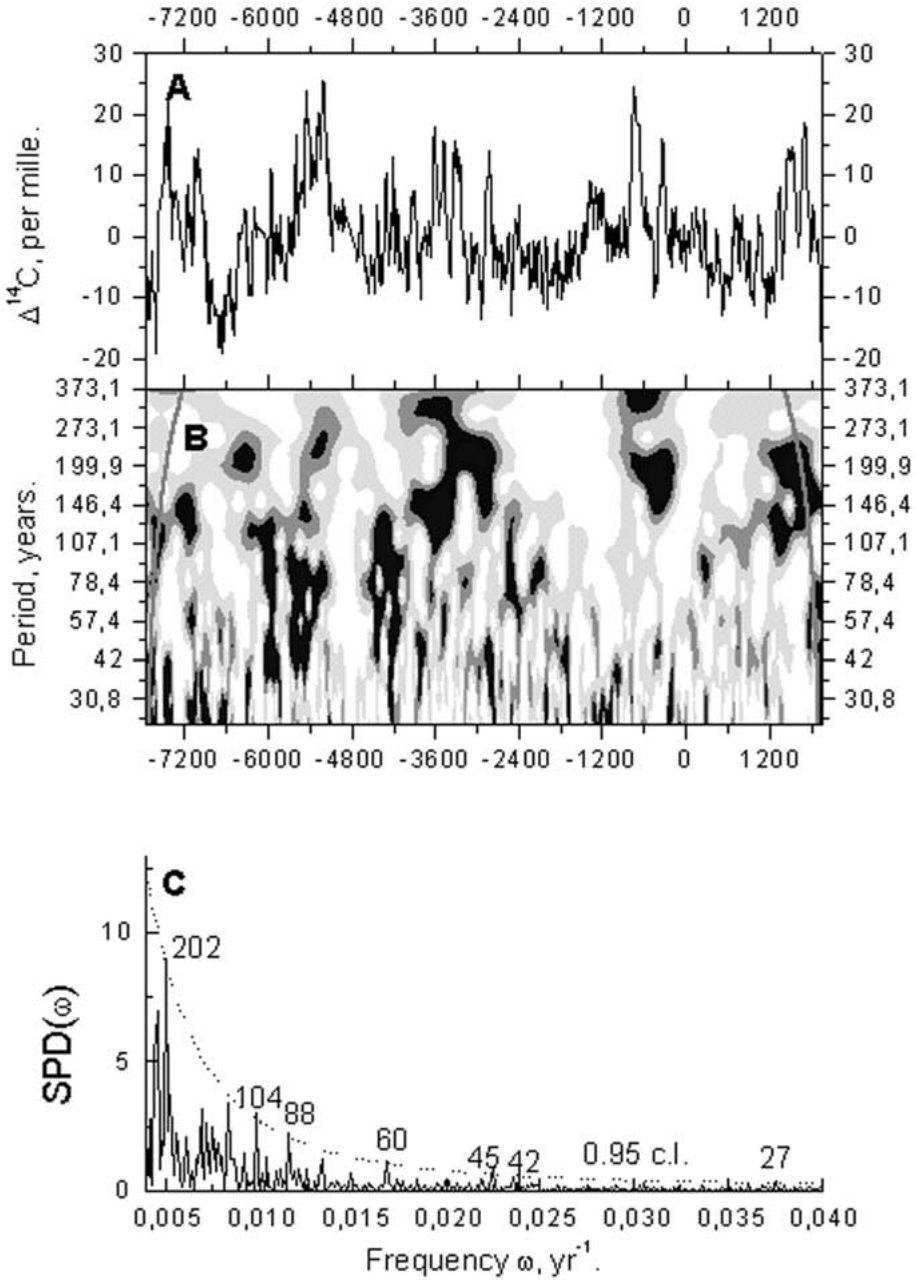

Figure 6. (A) Residuals of long decadal $\Delta^{14}C$ record of Stuiver and Pearson (1993). (B) Local wavelet (Morlet basis) spectrum of the residuals of long decadal $\Delta^{14}C$ record. *White domains* – local wavelet power < 0.2, *black domains* – local wavelet power > 1.0 (0.99 c.l.). (D) Fourier spectrum of the residuals of long decadal $\Delta^{14}C$ record. *Dotted line*: 0.95 c.l. (red noise factor 0.9).

TABLE I
Secular variations in different solar activity indicators.

Data set	Time interval	Gleissberg frequency band		Suess frequency band
		50–80 yrs	90–140 yrs	(160–260 yrs)
Wolf number	1700–1995 AD	Strongly manifested	Strongly manifested	?
GSSN	1700–1995 AD	Distinctly manifested	Strongly manifested	?
SONE 1	0–800 AD	Manifested, but weakly significant	Manifested but weakly significant	Manifested but weakly significant
SONE 2	801–1801 AD	Absent	Manifested, but weakly significant	Distinctly manifested
^{10}Be	1000–1900 AD	Distinctly manifested	Strongly manifested	Distinctly manifested
Wolf number (reconstructed)	1100–1995 AD	Strongly manifested	Strongly manifested	Strongly manifested
Δ^{14}C	7748 BC–1945 AD	Appears periodically	Appears periodically	Appears periodically

cosmic rays (see, for example, Dergachev and Veksler, 1991). This means that this epoch was a period of strong influence by cosmic rays. The more pronounced ^{14}C variability in the 40–270-year range during 2500–6000 B.C. is a proof for its solar origin. It can also be noted that periods of amplification of the Suess cycle ($\approx$1600 A.D., $\approx$400 B.C., $\approx$3100 B.C., $\approx$5300 B.C., see Figure 6(b)) coincide with the maxima of the ca. 2400-year Hallstattzeit cycle that have been found already by Vasiliev, Dergachev, and Raspopov (1999). The red noise factor for the long decadal ^{14}C series was 0.9.

The information extracted from a variety of indicators of SA is summarized in Table I.

It is seen from Table I that variations with periods 50–80 years, 90–140 years and 160–260 years are clearly observed in different SA data (both direct and proxy) including indicators of sunspot and auroral activity and solar modulation of GCR. It proves the existence of all these modes of the Sun's variability over a time scale of 1000 years and more. Hence, the time variations, mentioned above, are likely connected with the oscillating system governing the SA fluctuations.

The ratio of periods of the main solar variations (50–80 years)/(90–140 years) ≈ (90–140 years)/(160–260 years) ≈ (1/2) is very interesting and may reflect fractal properties of SA. But the quality of our data on SA is not good enough to make any ultimate conclusion about the nature of the solar oscillator. For example, the data on Wolf numbers, both directly measured and derived from aurorae observations, show that 50–80 and 90–140-year modes rather replace each other and alternate (see Figures 2 and 5(b)) but in the cosmogenic isotope data these cycles can exist simultaneously (see Figures 4(b) and 6(b)). So, various indicators of SA give us a different picture about the time evolution of the main modes of solar variability, while precise information on this point is very important for understanding of fractal and other properties of activity of the Sun. Hence, further investigations of changes of SA over time scales as long as possible, are necessary.

The next question is connected with a possibility of solar-climate link, which is actively debated. Modern methods of dendrochronology make it possible to obtain climatic proxies with a length up to 1000 years and more and, hence, to extract information about climate change over a long time scale. Here we analysed the annual northern hemisphere temperature reconstruction of Mann, Bradley, and Hughes (1999), which is presented in Figure 7 together with its Fourier and wavelet spectra (red noise factor was 0.25). As seen from Figures 7(b) and 7(d) highly significant time variations with periods ≈ 200, 110–120, and 50–80 years exist in the temperature proxy of Mann, Bradley, and Hughes (1999). These periodicities are very similar to those established in SA. Records of global northern hemispheric temperature and ^{10}Be in South Pole ice, wavelet filtered in the 56–194-year scale band, are plotted in Figure 7(c). Some negative correlation between these series (coefficient of correlation 0.51) is seen at least during the last 700 years. It gives us new evidence of long-term solar activity having an influence on climate. The question about the centennial solar modulation of global and regional terrestrial climate and its possible mechanisms have been discussed in more detail by Ogurtsov *et al.* (2001, 2002).

5. Conclusions

Summarising results of our analysis we can conclude that:

(1) Two basic modes of long-term solar variability – the cycles of Gleissberg and Suess – really exist at least within the last millennium, and probably during a longer period (up to 10 000 last years). They are manifested in direct and proxy indicators of different parameters of solar activity (sunspots, heliospheric solar modulation, aurorae). It indicates that Gleissberg and Suess cycles are the fundamental features of SA.

(2) The century-type solar variation – the Gleissberg cycle has not a single 80–90-year periodicity (as it was considered till now) but has a wide frequency band (50–140 years) and a complex character. More likely it consists of two oscillation

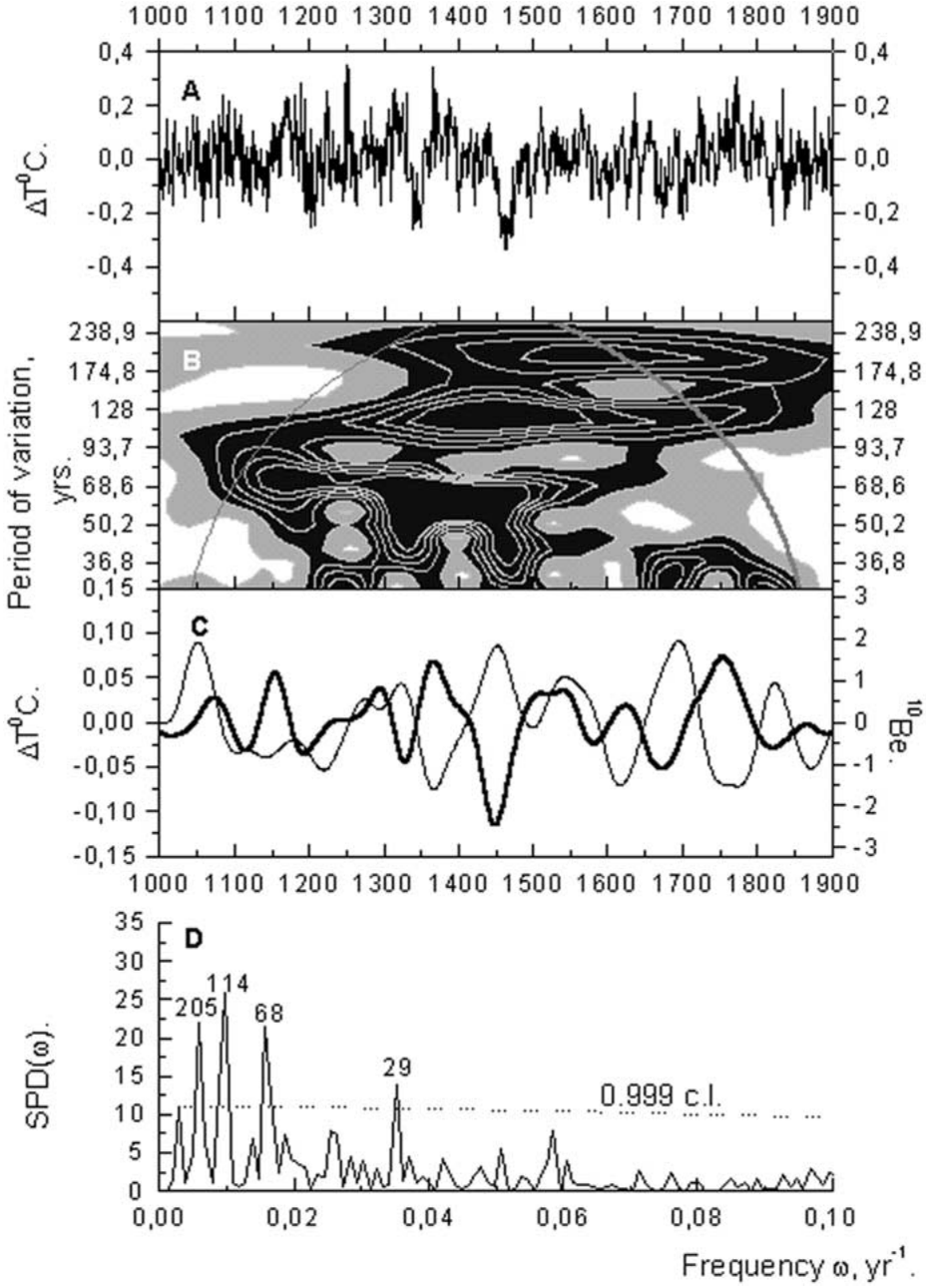

Figure 7. (A) Mean annual temperature in the northern hemisphere, reconstructed by Mann *et al.* (1999). (B) Local wavelet (Morlet basis) spectrum of the temperature multiproxy of Mann *et al.* (1999). *White domains* – local wavelet power < 0.2, *black domains* – local wavelet power > 1.0 (0.99 c.l.). (C) Temperature multiproxy of Mann *et al.* (1999) and ^{10}Be concentration at the South Pole, wavelet filtered (MHAT basis) in 56–194 scale band. (D) Fourier spectrum of the temperature multiproxy of Mann *et al.* (1999). *Dotted line*: 0.999 c.l. (red noise factor 0.25).

modes – 50–80-years periodicity and 90–140-years periodicity. The Suess cycle is 160–260 years and the cycle is more stable and less complex, as Schove (1983) suggested.

(3) Global northern hemisphere climate has appreciable variability in the Gleissberg and Suess bands at least during the last 1000 years. It confirms an assumption that climate is modulated by SA during the corresponding time interval.

The work made in this paper using modern statistical methods shows that complex analysis of all variety of direct and indirect information about SA in the past is a perspective tool for investigation of long-term variability

Acknowledgements

This research was done in the context of an exchange between the Russian and Finnish Academies (project No. 16) and was supported by INTAS grant No. 2002-550. Yu. A. Nagovitsyn is grateful to the Federal program 'Astronomy' (1–5.13) and INTAS (grant Nos. 2001-543, 2001-752). M. G. Ogurtsov is grateful to S. Helama for his aid in the preparation of the paper.

Appendix 1. Estimation of Significance of Wavelet Spectra

One of the more important questions of wavelet analyses is the estimation of significance of details of the calculated spectra. Recently, Torrence and Compo (1998) suggested a perspective method for the solution of the problem. They recommended to do this evaluation on the basis of a comparison of normalised local wavelet spectrum of analysed signal with some kind of background spectrum. However, the next task arises at once – a problem to choose the appropriate background spectrum. Our analysis showed that the use of a pure noise spectrum as a background is not the best way and may lead to underestimation of significance at least in a case when the signal is corrupted by noise. In the present work we therefore followed the approach of Torrence and Compo (1998) but used a number of background global wavelet spectra of artificial signals, each of which consisted of a sinusoid with fixed period and Gaussian red noise and with a fixed significance X. Here we illustrate our method by means of a test time series of 900 points, consisting of two sinusoids with the periods 7.8 year and 73.0 year and of Gaussian red noise with $\alpha = 0.3$ (Figure 8(a)). Both these sinusoids are highly significant, as is confirmed in the Fourier spectrum (Figure 8(b)). The 0.999 confidence level (c.l.) in Figure 8(b) was calculated as multiplication of the usual red noise continuum by a corresponding χ^2 value (6.4 for 0.999). The X confidence level for the global wavelet spectrum of signal under investigation was calculated in the following way:

(1) Initially we calculated parameters of the signal $Y^X(t, \omega_k)$, which has unit variance and consists of red (AR(1)) noise and a sinusoid with frequency ω_k, so

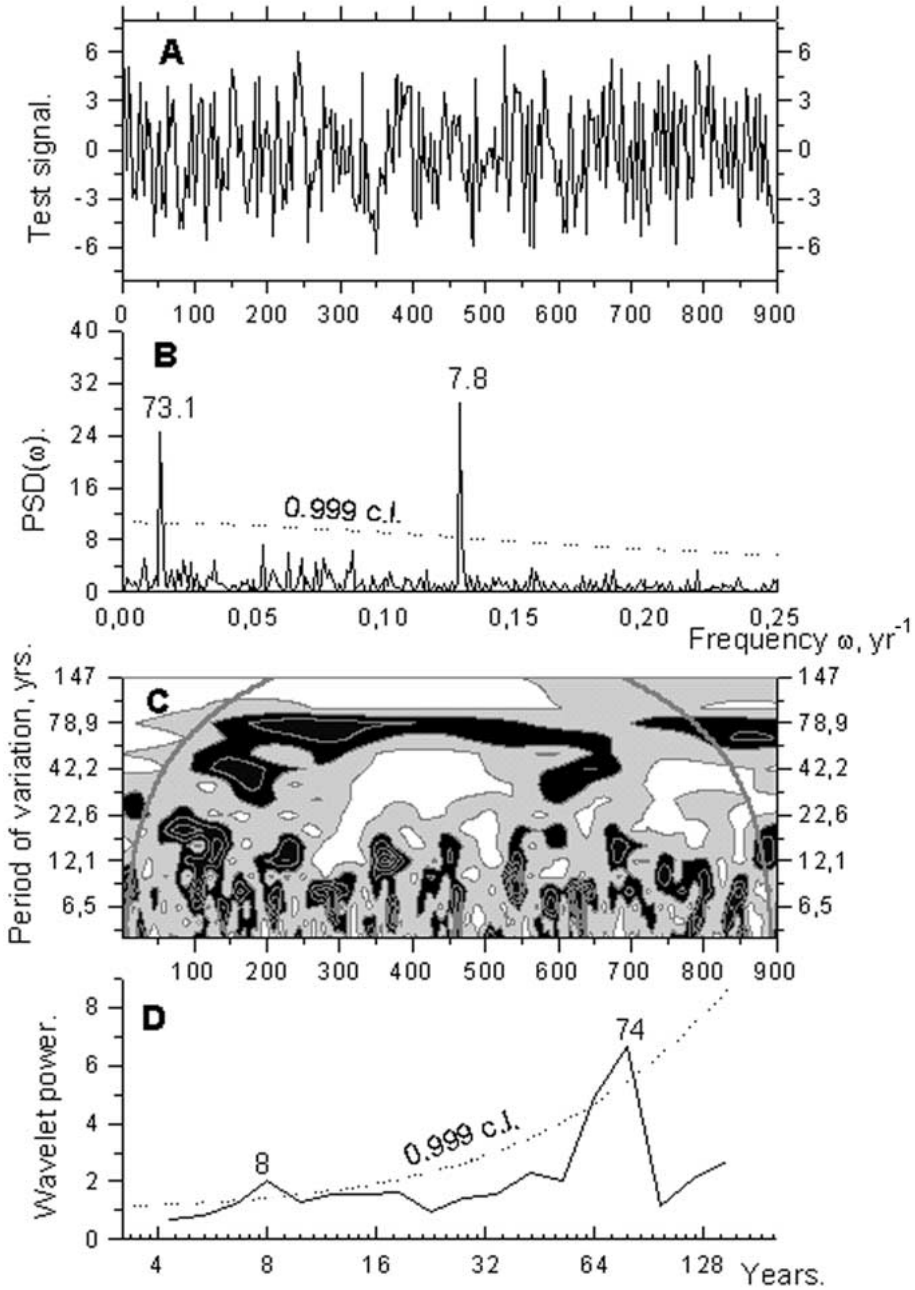

Figure 8. (A) Test signal contains two sinusoids (with periods 73 yr and 8 yr) corrupted by red noise with $\alpha = 0.3$. (B) Fourier spectrum of the test signal. (C) Local wavelet (Morlet basis) spectrum of the test signal. *White domains* – local wavelet power < 0.2, *black domains* – local wavelet power > 1.0 (0.999 c.l.). (D) Global wavelet (Morlet basis) spectrum of the test signal.

that the peak of its Fourier spectrum has a X confidence level. It means that for the signal

$$Y^X(t, \omega_k) = A_0^X(\omega_k)\ \cos(\omega_k t) + R^\alpha(t), \tag{1}$$

where $R^\alpha(t)$ is a red noise with a factor α and variance σ_r^2, $A_0^X(\omega_k)$ is to be calculated so that $P_N(\omega)$ – the normalized Fourier spectrum of $Y^X(t, \omega_k)$ – at the frequency ω_k will have the peak $P_N^X(\omega_k)$ with the confidence level X, i.e.,

$$P_N^X(\omega_k) = P_R^\alpha(\omega_k)\frac{\chi_{2,X}^2}{2}, \tag{2}$$

where

$$P_R^\alpha(\omega) = \frac{1-\alpha^2}{1+\alpha^2-2\cos\left(\dfrac{\omega}{N_0}\right)} \quad \text{is a spectrum of red noise,} \tag{3}$$

$\chi_{2,X}^2$ is the value of χ_2^2 corresponding to the chosen confidence level X, N_0 is number of points in the data set. It is easy to calculate $A_0^X(\omega_k)$. According to Horne and Baliunas (1986) for the signal consisting of a sinusoid and normally distributed random value with the zero mean we have

$$P_N^X(\omega_k) = \frac{N_0}{2}\frac{A_0^X(\omega_k)^2}{\dfrac{A_0^X(\omega)^2}{2} + \sigma_r^2}. \tag{4}$$

If we work with the signal initially normalized by its variance, i.e.,

$$\frac{A_0^X(\omega_k)^2}{2} + \sigma_r^2 = 1, \tag{5}$$

then

$$A_0^X(\omega_k) = \sqrt{\frac{2P_N^X(\omega_k)}{N_0}}. \tag{6}$$

(2) At the next step a number N_s of Monte-Carlo simulations is performed. In each simulation a signal $Y^X(t, \omega_k)$ is generated and a global Morlet wavelet spectrum of the signal is calculated. These N_s spectra are averaged and a final mean spectrum $\overline{P}_{W,X}(a, \omega_k)$ is determined. Apparently the spectrum $\overline{P}_{W,X}(a, \omega_k)$ has a maximum $P^{\max}(a_k)$ at $a_k = 1/\omega k$. In Figures 9(a) and 9(b) the mean global wavelet spectra, for $\omega_3(a_3 = 18$ year) and $\omega_8(a_3 = 70$ year), are shown with thick lines. The corresponding mean Fourier spectra are shown as thin lines.

(3) After this procedure has been carried out for a number of frequencies ω_1, ω_2, ..., ω_n (signals contain sinusoids with different frequencies) a number of maxima of global Morlet wavelet spectra $P^{\max}(a_1)$, $P^{\max}(a_2)$, ..., $P^{\max}(a_n)$ will

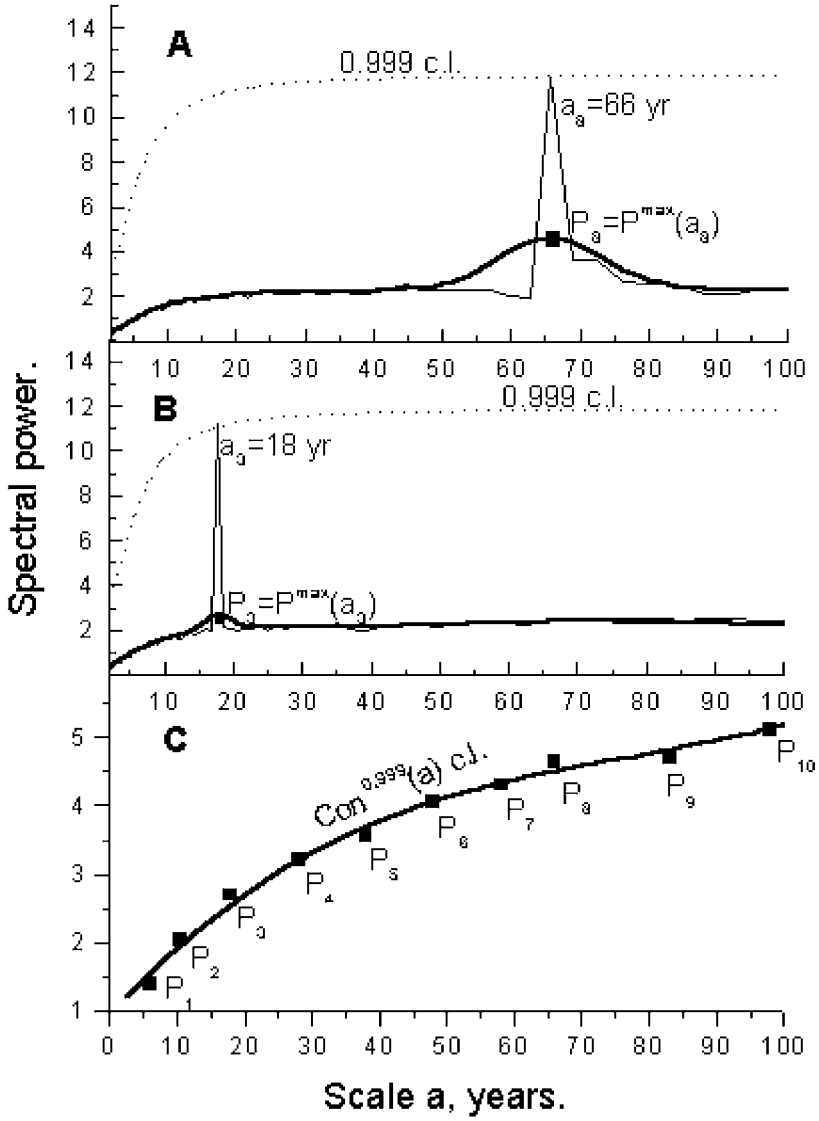

Figure 9. (A) Mean Fourier (*thin line*) and Morlet wavelet (*thick line*) spectra of signal consisting of 900 points and containing a sinusoid with period 66 years corrupted by red noise with $\alpha = 0.3$. Significance of 66 yr variation is 0.999. *Dotted line*: 0.999 c.l. for Fourier spectrum. (B) Mean Fourier (*thin line*) and Morlet wavelet (*thick line*) spectra of signal consisting of 900 points containing a sinusoid with period 18 years corrupted by red noise with $\alpha = 0.3$. Significance of 18 year variation is 0.999. *Dotted line*: 0.999 c.l. for Fourier spectrum. (C) 0.999 confidence level (*thick line*) for Morlet wavelet spectrum of a signal consisting of 900 points.

be obtained. Finally, joining the points $P^{\max}(a_1)$, $P^{\max}(a_2)$, ..., $P^{\max}(a_n)$ we defined a curve $Con^X(a)$ - the X confidence level for the global wavelet spectrum of the time series consisting of N_0 points (see Figure 9). This line was used as a background spectrum in further analyses of local spectra, i.e., all domains of the local wavelet spectrum of the analysed signal (consisting of N_0 points), which lay above $Con^X(a)$, were considered as true features with the confidence level X. In the Figures 8(c) and 8(d) local and global wavelet spectra of tested signal are shown. The confidence level was estimated according to the method described above. The good agreement between the significance of peaks of Fourier and wavelet spectra (both global and local) is evident. It should be noted that if we used a pure red noise spectrum as background the significance of global wavelet spectrum peaks would be less than 0.99 and the same would be for the local spectrum.

Appendix 2. Function of Autosimilarity and Analysis of Binary Information

For the analysis of binary time series we used an approach, developed by Nagovitsyn (1992, 2001) and based on ideas from cluster analyses. Multidimensional statistics make it possible to classify events proceeding from an intuitively formulated concept of their similarity in a space of features. One of the more popular measures of similarity of cases i and j, having features $k = 1, 2, \ldots$, is the general similarity coefficient g_{ij}, suggested by Gower (1971):

$$g_{ij} = \frac{\sum_{k=1}^{p} U_{i\ jk}}{\sum_{k=1}^{p} W_{ijk}}, \tag{7}$$

where U_{ijk} denotes the contribution provided by the kth variable, W_{ijk-} are information weight factors. U_{ijk}, W_{ijk} are different for different kinds of data (quantitative, nominal or binary). In case of a binary variable we have:

Case i	+	+	−	−
Case j	+	−	+	−
U_{ijk}	1	0	0	0
W_{ijk}	1	1	1	0

If we are interested in periodicities contained in p-dimension time series, we can formulate a concept for a function of autosimilarity (AF) – a measure of similarity of a matrix of the data (time $*$ features) with itself when shifted by time τ:

$$g(\tau) = \frac{1}{n - \tau + 1} \sum_{i=0}^{n-\tau} \left(\sum_{k=1}^{p} U_{i,i+\tau,k} / W_{i,i+\tau,k} \right). \tag{8}$$

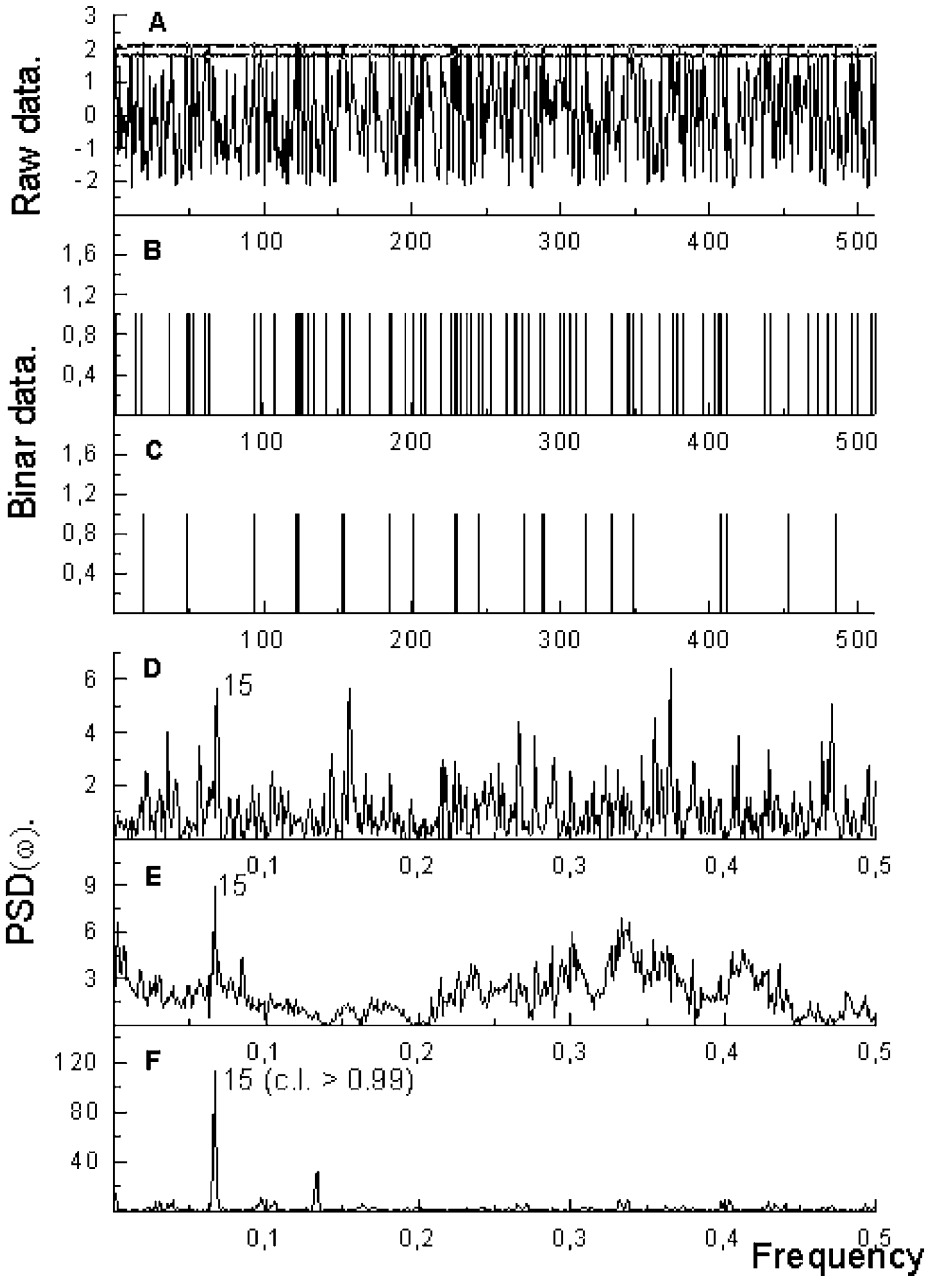

Figure 10. (A) Test series, consisting of a sinusoid with a period of 15 years, corrupted by strong white noise. *Thick grey lines* – 1.75 and 2.05 levels. (B) Binary series made from the initial one using 1.75 threshold. (C) Binary series made from the initial one using 2.05 threshold. (D) Fourier spectrum of the initial series, plotted in (A). (E) Fourier spectrum of the binary series, plotted in (B). (F) Fourier spectrum of the binary series, plotted in (C).

It is seen that the autosimilarity function $g(\tau)$ can be considered as a multidimensional analogue of the autocorrelation function. Its first important advantage is its applicability for analysis of different types of variable, including a binary one. AF has been applied for analysis of multidimensional data (Nagovitsyn, 1992) and in present paper we used its one-dimensional version. The second useful property of the AF is the possibility to use it for the analysis of extreme events. This opportunity is illustrated in Figure 10. A time series $Y(t)$, constructed of a sinusoid with period 15 years and white noise is shown in Figure 10(a). The sinusoid is so strongly corrupted by noise that its Fourier spectrum (Figure 10(d)) does not contain any significant peak. Then we constructed a binary series $Y^B(t)$ from $Y(t)$ by a rule

$$\begin{cases} Y^B(t) = 1, Y(t) > Y_{\text{thrs}}, \\ YB(t) = 0, Y(t) < Y_{\text{thrs}}. \end{cases} \tag{9}$$

We made two binary data sets using two thresholds Y_{thrs} – a low one (1.75) and a high one (2.05). These binary series (the first consists of 80 events and the second of 22 events) are shown in Figures 10(b) and 10(c) and the corresponding Fourier spectra of their autosimilarity functions are plotted in Figures 10(e) and 10(f). The significance of the peak of the Fourier spectrum of AF was estimated by means of a statistical experiment. In this experiment a number of randomly distributed copies of the analysed data set were constructed (see Bieber *et al.*, 1990) and the Fourier spectrum of AF of each of these copies was calculated. Then the value of the strongest peak of the spectrum of each random set was determined and compared with the peak under investigation. If the main peak of the noisy series was higher than the analysed peak, the test was considered as having a positive result. Significance of the peak, of interest to us, was finally estimated as a ratio of positive results to full number of simulations. It is seen from Figures 10(e) and 10(f) that analyzing a binary series consisting of extreme events allows one to suppress noise substantially and to reveal the variation, which cannot be found in the initial data. The SONE time series, investigated in the present work, is just an example of an extreme event record. Really, giant sunspots available for observation by the unaided eye can occur mainly during the periods of high SA. According to Eddy, Stephenson, and Yau (1989) the Wolf number R_Z must exceed 50 in order that so large a sunspot or sunspot group could appear.

References

Astafieva, N. M.: 1996, *UFN* **166**, 1145 (in Russian).

Bard, E, Raisbeck, G. M., Yiou, F., and Jouzel, J.: 1997, *Earth Planetary Sci. Lett.* **150**, 453.

Beer, J., Siegenthaler, U., Bonani, G., Finkel, R. C., Oeschger, H., Suter, M., and Wölfi, W.: 1988, *Nature* **331**, 675.

Beer, J., Blinov, A., Bonani, G., Finkel, R. C., Hofman, H. J., Lehmann, B., Oeshger, H., Siggl, A., Schwander, J., Staffelbach, T., Stauffer, B., Suter, M., and Wölfli W.: 1990, *Nature* **347**, 164.

Beer, J., Soos, F., Lukachyk, Ch., Mende, W., Rodrigues, J., Siegenthaler, U., and Stellmacher, R.: 1994, *NATO ASI Series* **25**, 221.
Bieber, J. W., Secker, D., Stanev, T., and Steigmer, G.: 1990, *Nature* **348**, 407.
Chistyakov, V. F.: 1986, *Soln. Data* No. 6, 78 (in Russian).
Cole, T. W.: 1973, *Solar Phys.* **30**, 103.
Damon, P. E.: 1970, in I. U. Olsson (ed), *Radiocarbon Variations and Absolute Chronology, Proc. of Nobel Symposium* **12**, 571.
Damon, P. E. and Peristykh, A. N.: 1997, in R. Boström *et al.* (eds.), *IAGA 1997 Abstract Book,* Reklam & Katalogtryk, Uppsala, Sweden, 191.
Dergachev, V. A. and Veksler, V. S.: 1991, *Application of Radiocarbon Method for the Investigation of Past Nature*, Leningrad, 255 pp. (in Russian).
Eddy, J. A.: 1976, *Science* **192**, 1189.
Eddy, J. A., Stephenson, F. R., and Yau, K. K. C.: 1989, *Royal Astron. Soc., Quat. J.* **30**, 65.
Gleissberg, W.: 1944, *Terrest. Mag.* **49**, 243.
Gower, J. C.: 1971, *Biometrics* **27**, 857.
Horne, J. H. and Baliunas, S. L.: 1986, *Astrophys. J.* **302**, 757.
Hoyt, D. V. and Schatten, K.: 1998, *Solar Phys.* **179**, 189.
Lal, D.: 1987, *Geophys. Res. Lett.* **14**, 785.
Mann, M. E., Bradley, R. S., and Hughes, M. K.: 1999, *Geophys. Res. Lett.* **26**, 759.
Monaghan, M. C.: 1987, *Earth Planetary Sci. Lett.* **84**, 197.
Nagovitsyn, Yu. A.: 1992, *Space-Temporal Aspects of Solar Activity*, A.F., Ioffe PhTI, St.-Petersburg, pp. 197–208.
Nagovitsyn, Yu. A.: 1997, *Astron. Lett.* **23**, 742.
Nagovitsyn Yu. A: 2001, *Geomagn. Aeron.* **41**, 711.
Ogurtsov, M. G., Kocharov, G. E., Lindholm, M., Eronen, M., Merilainen, J., and Nagovitsyn, Yu. A.: 2002, *Solar Phys.* **205**, 403.
Ogurtsov, M. G., Kocharov, G. E., Lindholm, M., Eronen, M., Merilainen, J., and Nagovitsyn, Yu. A.: 2002, *Holocene*, submitted.
Peristykh, A. N. and Damon, P. E.: 2000, *Radiocarbon* **42**, 137.
Schove, D. J.: 1979, *Solar Phys.* **63**, 423.
Schove, D. J.: 1983, *Sunspot Cycles*, Hutchinson Ross Publ. Co., Stroudsburg, Pennsylvania.
Solanki, S. K., Schüssler, M., and Fligge, M.: 2000, *Nature* **408**, 445.
Stuiver, M. and Braziunas, T. F.: 1989, *Nature* **338**, 405.
Stuiver, M. and Braziunas, T. F.: 1993, *Holocene* **3**, 1.
Stuiver, M. and Pearson, P. J.: 1993, *Radiocarbon* **35**, 215.
Stuiver, M. and Quay, P. D.: 1980, *Science* **207**, 11.
Suess, H. E: 1980, *Radiocarbon* **22**, 200.
Torrence, C. and Compo, G. P.: 1998, *Bull. Am. Meteorol. Soc.* **79**, 61.
Vasiliev, S. S., Dergachev, V. A., and Raspopov O. M.: 1999, *Geomagn. Aeron.* **39**, 80 (in Russian).
Waldmeier, M.: 1961, *The Sunspot Activity in the Years 1610–1960*, Schulthess and Company AG, Zürich.
Wittmann, A.: 1978, *Astron. Astrophys.* **66**, 93.
Wittmann, A. D. and Xu, Z.: 1987, *Astron. Astroph. Suppl. Ser.* **70**, 83.
Willis, D. M, Easterbrook, M. G., and Stephenson, F. R.: 1980, *Nature* **287**, 617.
Yunnan Observatory: 1977, *Chinese Astron.* **1**, 347.